



Article

Influence of a Physiologically Formed Blood Clot on Pre-Osteoblastic Cells Grown on a BMP-7-Coated Nanoporous Titanium Surface

Leonardo Raphael Zuardi ¹, Cleide Lúcia Araújo Silva ², Eduardo Magalhães Rego ², Giovana Vacilotto Carneiro ¹, Silvia Spriano ³, Antonio Nanci ⁴ and Paulo Tambasco de Oliveira ^{1,*}

¹ Department of Basic and Oral Biology, School of Dentistry of Ribeirão Preto, University of São Paulo, Ribeirão Preto 14040-904, SP, Brazil

² Haematology Division, Ribeirão Preto Medical School, University of São Paulo, Ribeirão Preto 14051-060, SP, Brazil

³ Department of Applied Science and Technology, Politecnico di Torino, 10129 Torino, Italy

⁴ Faculté de médecine dentaire, Université de Montréal, Montréal, QC H3T 1J4, Canada

* Correspondence: tambasco@usp.br; Tel.: +55-16-99623-3663

Abstract: Titanium (Ti) nanotopography modulates the osteogenic response to exogenous bone morphogenetic protein 7 (BMP-7) in vitro, supporting enhanced alkaline phosphatase mRNA expression and activity, as well as higher osteopontin (OPN) mRNA and protein levels. As the biological effects of OPN protein are modulated by its proteolytic cleavage by serum proteases, this in vitro study evaluated the effects on osteogenic cells in the presence of a physiological blood clot previously formed on a BMP-7-coated nanostructured Ti surface obtained by chemical etching (Nano-Ti). Pre-osteoblastic MC3T3-E1 cells were cultured during 5 days on recombinant mouse (rm) BMP-7-coated Nano-Ti after it was implanted in adult female C57Bl/6 mouse dorsal dermal tissue for 18 h. Nano-Ti without blood clot or with blood clot at time 0 were used as the controls. The presence of blood clots tended to inhibit the expression of key osteoblast markers, except for *Opn*, and rmBMP-7 functionalization resulted in a tendency towards relatively greater osteoblastic differentiation, which was corroborated by runt-related transcription factor 2 (RUNX2) amounts. Undetectable levels of OPN and phosphorylated suppressor of mothers against decapentaplegic (SMAD) 1/5/9 were noted in these groups, and the cleaved form of OPN was only detected in the blood clot immediately prior to cell plating. In conclusion, the strategy to mimic in vitro the initial interfacial in vivo events by forming a blood clot on a Ti nanoporous surface resulted in the inhibition of pre-osteoblastic differentiation, which was minimally reverted with an rmBMP-7 coating.

Keywords: BMP-7; osteoblast; titanium; nanotopography; blood clot



Citation: Zuardi, L.R.; Silva, C.L.A.; Rego, E.M.; Carneiro, G.V.; Spriano, S.; Nanci, A.; de Oliveira, P.T. Influence of a Physiologically Formed Blood Clot on Pre-Osteoblastic Cells Grown on a BMP-7-Coated Nanoporous Titanium Surface. *Biomimetics* **2023**, *8*, 123. <https://doi.org/10.3390/biomimetics8010123>

Academic Editors: Monica Dettin and Annj Zamuner

Received: 6 February 2023

Revised: 10 March 2023

Accepted: 13 March 2023

Published: 16 March 2023



Copyright: © 2023 by the authors. Licensee MDPI, Basel, Switzerland. This article is an open access article distributed under the terms and conditions of the Creative Commons Attribution (CC BY) license (<https://creativecommons.org/licenses/by/4.0/>).

1. Introduction

The functionalization of biomaterial surfaces with bioactive molecules is considered a promising strategy when specific cellular and/or tissue biological effects are desired [1,2]. An evaluation of the effectiveness of these surface modifications through clinical tests follows previous in vitro analyses and in vivo studies in animal models [3,4]. In vitro studies on the biological characterization of functionalized biomaterials have been developed using two- and three-dimensional cell culture models, which, at least theoretically, explain the complex phenomena of cell interactions in the context of interfacial tissue formation in a controlled environment [3,5]. However, importantly, most of these in vitro models do not take into account the formation of a physiological blood clot, simultaneously and/or prior to the adhesion and spreading of different cell types on the biomaterial surface. The addition of the formation of a three-dimensional fibrin clot to the model and the presence of functional leukocytes, platelets, plasma proteins, and proteases reduce the distance between the in vitro biological characterization and the in vivo reality of animal models and clinical tests [6,7].

Bone morphogenetic protein 7 (BMP-7) has been used in functionalization studies of biomaterials, due to its recognized stimulatory effects on osteogenic activity under specific conditions and the permission for its use in humans by the Food and Drug Administration [8,9]. The strategies used to functionalize with BMP-7 involve modifications of the biomaterial surface chemistry and topography at a nanoscale, including those of metals [8–11]. In a previous initial study, we observed that the effects of providing 40 and 200 ng/mL of a recombinant mouse (rm) BMP-7 to osteoblastic cells grown on titanium (Ti) were modulated by the nanotopographic features of its surface, with an increased expression of the osteoblast markers osteopontin (OPN) and alkaline phosphatase (ALP), but without enhancement in the mineralized matrix formation [12]. Interestingly, the Ti nanotopography (Nano-Ti) per se (without rmBMP-7 in the culture medium) promoted osteogenic differentiation compared with an almost flat surface at a nanoscale [12]. Based on these results, we designed the present study aiming to evaluate the effects of rmBMP-7-functionalized Nano-Ti on *in vitro* osteoblastic differentiation when a physiological blood clot is formed prior to the cell culture analyses.

We tested whether the presence of a blood clot alters key aspects of the interaction of osteoblastic cells with the nanotopographic surface with or without rmBMP-7 coating. As reported in the literature, the majority of studies that evaluate the interactions of blood clots with biomaterials use the simple addition of blood on their surfaces [13–17]. The present study goes further by including the formation of a physiological blood clot using the surgical approach proposed elsewhere [18] and adapted to our conditions to ensure the implant placement in a mouse dorsal dermal tissue model. The implant Ti discs were chemically treated with a mixture of sulfuric acid (H₂SO₄) and hydrogen peroxide (H₂O₂) to create a highly hydrophilic, biomimetic TiO₂ nanotopography [19] supportive of (i) functionalization with organic molecules by physisorption [20] and (ii) osteogenic differentiation [12,21]. The average roughness of Nano-Ti has been reported to be on the order of 9 nm, with nanopore depths ranging from 5 to 25 nm [22,23]. The implant Ti discs were structured to limit the displacement of the blood clot.

2. Materials and Methods

2.1. Preparation of a Nanotopographic Titanium Surface (Nano-Ti)

To obtain Nano-Ti, commercially pure grade 2 Ti discs (Realum, São Paulo, Brazil), modified to exhibit a hollowed surface (Figure S1), were cleaned by sonication and etched in a solution consisting of equal volumes of concentrated 30% H₂O₂ and H₂SO₄ (95–97%) for 4 h (10 mL/disc) at room temperature (RT) [12,20]. Then, they were rinsed in distilled water, air dried, and autoclaved.

2.2. Functionalization of rmBMP-7 on Nano-Ti

Autoclaved Nano-Ti discs were incubated overnight at 4 °C in a solution of 400 ng/mL of rmBMP-7 (BP-5666, R&D Systems, Minneapolis, MN, USA), 0.1% BSA, and 4 mM HCl, and then washed three times with PBS at 37 °C [24].

2.3. Physiological Blood Clot Formation on Nano-Ti

The experimental protocol was approved by the Ethics Committee for the Use of Animals of Ribeirão Preto Medical School (FMRP-USP, Ribeirão Preto, Brazil), registered under the number 173/2016 (Figure S2). Female mice of the C57Bl/6 strain, GFP-positive, aged between 8 and 12 weeks, were used. The surgical model proposed by this study was based on Monroe and Hoffman [18], with adaptations. The animals were anesthetized with 3% isoflurane in an induction chamber, reaching a deep anesthetic, shaved on the posterior dorsal region, followed by antisepsis with povidone iodine (PVPI). A 250 mm incision was then made in the animal's skin in the sagittal plane region and the muscular fascia was ruptured to facilitate hemorrhage. Thus, two Nano-Ti discs (functionalized with or without rmBMP-7) were introduced on both sides in the subcutaneous regions of each animal with the side of the hollowed surface facing the hemorrhage. The incision was stapled using

veterinary surgical stapling (Autoclip 9 mm, Clay Adams, Vernon Hill, IL, USA). During and 6 h after surgery, the animals received a 40 mg/kg dose of the analgesic tramadol hydrochloride (Agener União, São Bernardo do Campo, Brazil), intraperitoneally (IP). After 18 h of blood clot formation, the animals were anesthetized with the administration of 5 mg/kg of 2% lidocaine hydrochloride (Lidovet, Engenho Novo, Brazil) IP and were sacrificed by a 150 mg/kg overdose of anesthetic with 1 g of sodium thiopental (Cristália, Itapira, Brazil) IP in order to remove the blood-clot-coated Nano-Ti discs. The discs and animals were organized into their intended respective groups, as shown in Table 1.

Table 1. Descriptive table of the number of animals and discs per group and per analysis. Western blotting (WB); real-time polymerase chain reaction (real-time PCR); morphology (epifluorescence and scanning electron microscopy).

| Groups | Animals per Group | Animals per Analysis | Discs per Analysis |
|-------------------------|-------------------|----------------------|---------------------------------------|
| MC3T3-E1 | - | - | |
| MC3T3-E1 + BMP-7 | - | - | |
| Clot * | 20 | WB (10) PCR (8) | WB (20) PCR (16) Morphology (4) |
| Clot + MC3T3-E1 | 20 | | |
| Clot + MC3T3-E1 + BMP-7 | 20 | Morphology (2) | |
| TOTAL | 60 | 60 | 200 |

* Additional 2 animals/4 BMP-7-coated Nano-Ti discs were used for morphological analyses of the Clot + BMP-7 group.

2.4. Pre-Osteoblastic MC3T3-E1 Cell Culture

The mouse pre-osteoblastic MC3T3-E1 cells, subclone 14 (CRL-2594, ATCC, Manassas, VA, USA), were used for a culture period of 5 days. Briefly, the cells were grown in T-75 culture flasks (Corning Inc., Kennebunk, ME, USA) in a 16 mL expansion medium composed of α -MEM (Invitrogen, Carlsbad, CA, USA), supplemented with 1% penicillin–streptomycin (Sigma-Aldrich, Saint Louis, MO, USA) and 10% fetal bovine serum (Invitrogen) at 37 °C in a humidified atmosphere containing 5% CO₂. After subconfluence, the cells were removed with 1 mM ethylenediaminetetraacetic acid EDTA (Gibco, Grand Island, NY, USA) and 0.25% trypsin (Gibco), plated at a density of 5×10^4 cells/well (~350 cells/mm²) on Nano-Ti discs placed in 24-well polystyrene plates (Corning Inc.), in an α -MEM culture medium supplemented with 5 μ g/mL ascorbic acid and 7 mM β -glycerophosphate (Sigma-Aldrich). At days 2 and 4 of culture, the culture medium was changed (1 mL/well), as previously reported [12].

2.5. Cell Morphology by Epifluorescence Microscopy

The samples (MC3T3-E1 cultures and the control blood clots) were fixed in 4% paraformaldehyde in a 0.1 M phosphate buffer (PB; pH 7.2) at RT and treated with Triton X-100 at 0.5% in PB to permeabilization, before being labeled with 1:200 Alexa Fluor 594-conjugated phalloidin (A12381, Invitrogen) and 300 nM 4',6-diamidino-2-phenylindole, dihydrochloride (DAPI, Molecular Probes, Eugene, OR, USA) [21]. The discs were mounted on glass slides (Thermo Fisher Scientific, Waltham, MA, USA) using a Vectashield anti-fade fluorescence mounting medium (Vector Laboratories, Burlingame, CA, USA). The images of the discs were acquired by an Axio Imager 2 fluorescence microscope (Carl Zeiss, Jena, Germany) using AxioVision 4.8.2 program, and processed in Adobe Photoshop CS6 (Adobe Systems, San Jose, CA, USA), as previously described [12].

2.6. Cell Morphology by Scanning Electron Microscopy (SEM)

The samples (MC3T3-E1 cultures and the control blood clots) were fixed in 2% glutaraldehyde (Electron Microscopy Sciences, Hatfield, UK) in a cacodylate buffer (0.9 mM Ca²⁺

and 0.5 mM Mg²⁺) for 2 h at RT, followed by two washes with 1% cacodylate buffer (EM Sciences) for 2 h at RT. Samples were then washed in Milli-Q water and incubated in saturated thiocarbohydrazide solution (Electron Microscopy Sciences) for 10 min at RT, followed by five washes in Milli-Q water and incubation in 1% OsO₄ (in Milli-Q water). The biological material was dehydrated in several baths with increasing concentrations of ethanol (30, 50, 70, 90, and 100%) and dried to the critical point with CO₂ (Bal-Tec CPD 030 Critical Point Dryer, Balzers, Liechtenstein). Then, the samples were fixed with silver glue (EM Science) on a metallic support and covered with gold (Bal-Tec CPD 050 Sputter Coater). The samples were analyzed using a JEOL JSM-6610LV scanning electron microscope (JEOL, Tokyo, Japan) at the Multiuser Laboratory of Electron Microscopy (LMME- FMRP-USP) using 20 and 25 kV.

2.7. Quantitative Real-Time Polymerase Chain Reaction (Real-Time PCR)

Briefly, the total RNA was removed using TRIzol LS (Invitrogen) and purified using the SV Total RNA Isolation System kit (Promega, Madison, WI, USA). Then, it was quantified in the GeneQuant 1300 device (GE Healthcare, Cardiff, UK) and assessed for its integrity using the 2100 Bioanalyser (Agilent, Santa Clara, CA, USA) (Figures S3 and S4). cDNA was synthesized from 1 µg of total RNA by reverse transcription using the High-Capacity cDNA Reverse Transcription kit (Applied Biosystems, Foster City, CA, USA), following the manufacturer's instructions. TaqMan probes (Applied Biosystems) (Table 2) were used to access the osteoblastic gene expression via the CFX96 device (Bio-Rad, Hercules, CA, USA), as previously detailed [12]. PCR reactions were performed in one biological replicate, resulting from the pooling of 16 independent wells/experimental replicates for each group, and with three technical replicates, at two different moments. The results were analyzed based on the value of the cycle threshold (Ct), and the normalization and relative quantification of the gene expression were performed by the 2^{-ΔΔCT} method [25]. The results were normalized by constitutive gene *Gapdh*, assigning 1 to the MC3T3-E1 group. No statistical testing was applied due to pooling [12].

Table 2. TaqMan probes used in real-time PCR analysis.

| Genes | Taqman Probes |
|--------------|---------------|
| <i>Runx2</i> | Mm00501584_m1 |
| <i>Osx</i> | Mm04933803_m1 |
| <i>Alp</i> | Mm00475834_m1 |
| <i>Bsp</i> | Mm00492555_m1 |
| <i>Oc</i> | Mm03413826_mH |
| <i>Opn</i> | Mm00436767_m1 |
| <i>Gapdh</i> | Mm99999915_g1 |

2.8. Western Blotting (WB)

Briefly, the samples were processed in an ultrasonic bath (Misonix, Farmingdale, NY, USA) using a RIPA buffer. The total protein was quantified using the micro Lowry assay using the DC™ kit protein assay (Bio-Rad). Then, proteins were separated by SDS polyacrylamide gel electrophoresis (10%) and transferred to polyvinylidene difluoride (PVDF) membranes (Thermo Fisher Scientific). The membranes underwent the following incubations at RT: (1) 5% skimmed milk or BSA solution in TBS-T, according to the manufacturer's recommendations; (2) primary monoclonal antibody anti-runt-related transcription factor 2 (RUNX2), 1:500 (#12556, Cell Signaling Technology Inc., Danvers, MA, USA); (3) primary anti-OPN monoclonal antibody MPIIB10-1, 1:1000 (Hybridoma Bank, Iowa City, IA, USA); (4) primary polyclonal anti-phosphorylated suppressor of mothers against decapentaplegic (SMAD) 1/5/9 antibody, 1:1000 (#13820, Cell Signaling Technology Inc.); (5) primary polyclonal anti-GAPDH antibody, 1:1500 (sc-25778, Santa Cruz Biotechnology, Dallas, TX, USA).

The membranes were analyzed in the G-Box (Syngene, Frederik, MD, USA). The number of band pixels was measured using GeneSys 1.6.9 (Syngene) and GeneTools 4.3.8 (Syngene), as previously detailed [12]. Western blotting was performed in one biological replicate, based on the pooling of 20 independent wells/experimental replicates for each group, and with one technical replicate. The results were normalized by constitutive protein GAPDH, assigning 1 to the MC3T3-E1 group. No statistical testing was applied due to the pooling [12].

3. Results

3.1. Epifluorescence and SEM Imaging

On day 5 of culture, MC3T3-E1 cells that were grown directly on Nano-Ti surfaces with or without rmBMP-7 functionalization were confluent, showing the beginning of multilayer formation and occasional mitotic figures (Figure 1A,B), exhibiting elongated shapes with occasional cytoplasmic projections (Figure 2A, arrows, and Figure 2B). Blood clot formation on Nano-Ti showed a complex structure, with an extensive three-dimensional fibrin network with which red blood cells, leukocytes, and platelets interacted (Figures 1C,D and 2C,D). These elements persisted with MC3T3-E1 culturing, but in smaller amounts compared with pre-osteoblastic cell layers. MC3T3-E1 cells maintained their elongated shapes when intermingled with the blood clot structure, showing larger cytoplasmic and nuclear dimensions compared with the GFP-positive leukocytes. Leukocytes and erythrocytes were clearly visible in the upper plane of the cultures (Figures 1E,F and 2E,F). Leukocytes exhibited either typical features of cell spreading, with cytoplasmic extensions, or a spherical morphology. No morphological changes that could be attributed to functionalization with rmBMP-7 were noticed in any of the groups (Figures 1 and 2, compare B with A, D with C, and F with E).

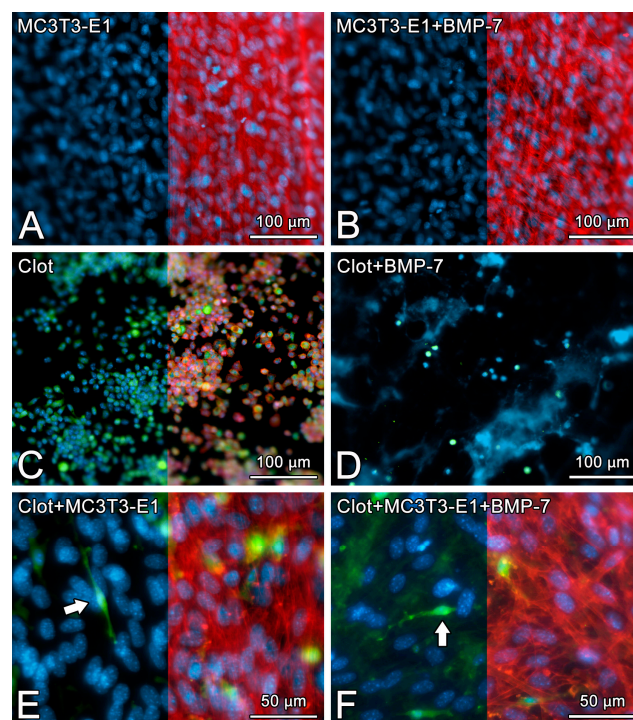


Figure 1. The epifluorescence of MC3T3-E1 cells on day 5 of culture (A,B), blood clot alone on time 0 (C,D), or the combination of both on day 5 of culture (E,F) on pristine Nano-Ti (A,C,E) or Nano-Ti functionalized with rmBMP-7 (B,D,F). Red fluorescence (Alexa Fluor 594 phalloidin) indicates the actin cytoskeleton (A–C,E,F), green fluorescence indicates the GFP-positive blood clot leukocytes (C–F), and blue fluorescence indicates the cell nuclei (DAPI nuclear stain) (A–F) and the fibrin network (D). Red fluorescence is deleted in the left halves of (A–C,E,F) using Adobe Photoshop CS6 for a better visualization of the cell nuclei and GFP-positive cells (white arrows in (E,F)) in the same microscopic field. Objectives: 20× (A–D); 40× (E,F).

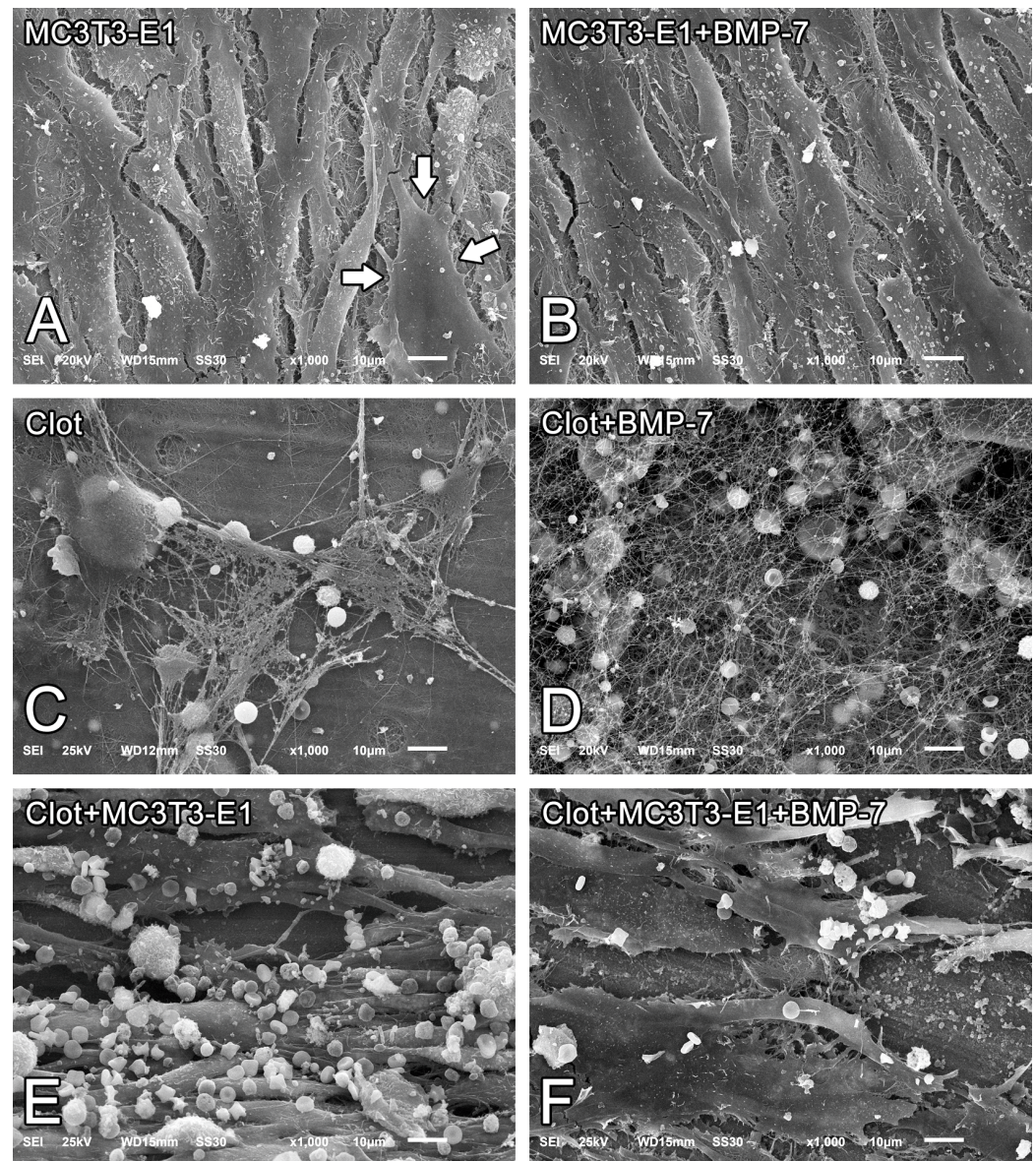


Figure 2. Scanning electron microscopy (SEM) imaging of MC3T3-E1 cells on day 5 of culture (A,B), blood clots alone on time 0 (C,D), or the combination of both on day 5 of culture (E,F) on pristine Nano-Ti (A,C,E) or Nano-Ti functionalized with rmBMP-7 (B,D,F). Original magnification: 1000 \times (A–F). MC3T3-E1 cells exhibit elongated shapes (white arrows in (A)) irrespective of the presence of a blood clot.

3.2. Quantitative mRNA Expression by Real-Time PCR

The results were presented as trends, as no statistical testing was applied due to the pooling of 16 independent experimental replicates for each group. The presence of blood clots altered the mRNA expression levels of key osteoblast markers in MC3T3-E1 cells grown on Nano-Ti, with a trend towards the inhibition of *Runx2*, osterix (*Osx*), *Alp*, bone sialoprotein (*Bsp*), and osteocalcin (*Oc*), except for *Opn*. Very low or minimal expression levels of these genes were detected in the clot group, while its *Opn* expression was high (Figure 3). Functionalization with rmBMP-7 resulted in a tendency towards a relatively small increase in the expression levels of these genes (about 0.3-fold for *Runx2*, 1.1-fold for *Osx*, 1.8-fold for *Alp*, and 4.8-fold for *Bsp*). The direct growth of MC3T3-E1 cells on Nano-Ti functionalized with rmBMP-7 supported lower *Runx2*, *Osx*, *Alp*, *Bsp*, and *Oc* levels compared with the ones on the pristine Nano-Ti (Figure 3).

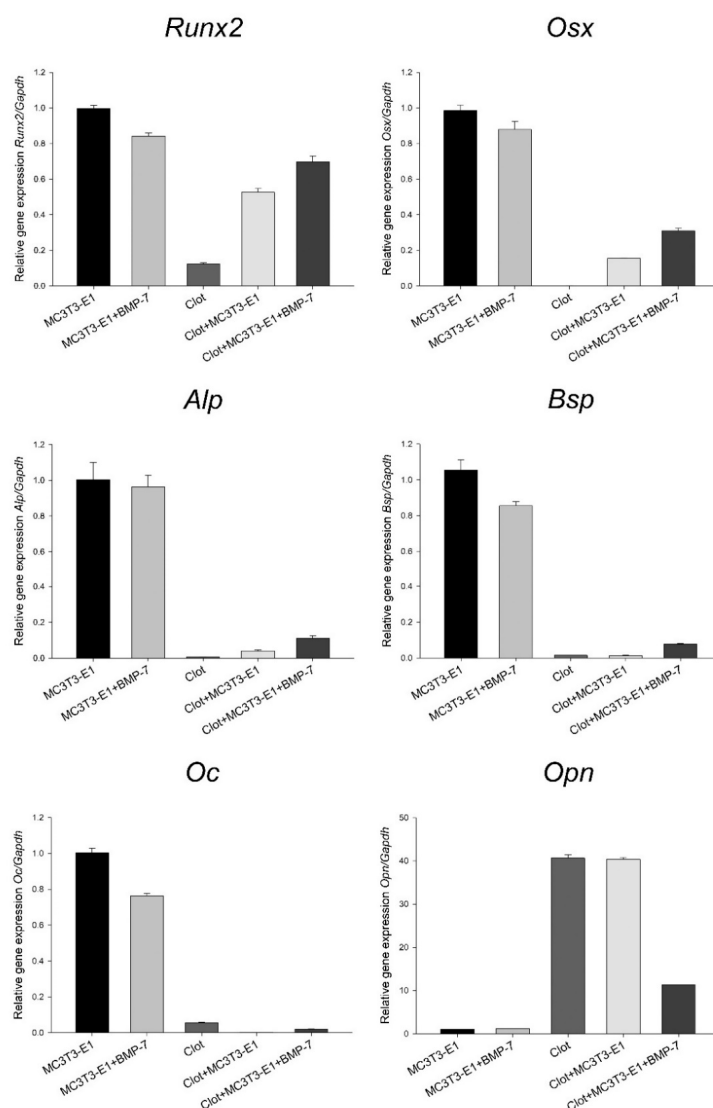


Figure 3. *Runx2*, *Osx*, *Alp*, *Bsp*, *Oc*, and *Opn* mRNA expression levels normalized to *Gapdh* in MC3T3-E1 cell cultures grown for 5 days and in blood clots on time 0 on Nano-Ti surfaces either functionalized with or without rmBMP-7. The bars represent one biological replicate (resulting from the pooling of 16 independent wells/experimental replicates for each group) run in three technical replicates (mean and SD). The mean value of the control MC3T3-E1 group is assigned a value of 1. Additional technical replicates obtained in a different moment using the same cDNA result in a similar expression pattern (Figure S5).

3.3. Protein Detection by WB

The results represented one technical replicate from the pooling of 20 independent experimental replicates for each group, and thus were presented as trends. An increase in RUNX2 was observed in MC3T3-E1 cells on Nano-Ti functionalized with rmBMP-7, irrespective of the presence of blood clots. Prior to cell plating, the blood clots showed no detectable amounts of RUNX2 (Figure 4A). An increase in OPN was detected in cultures grown on Nano-Ti coated with rmBMP-7 in the absence of blood clots, while no detectable amounts were noted when the cells interacted with blood clots pre-formed on rmBMP-7-coated Nano-Ti (Figure 4B). A cleaved form of OPN was only detected in the blood clots at time 0, immediately prior to cell plating (Figure 4B). The amounts of phosphorylated-SMAD 1/5/9 were reduced by about 20% in cultures grown on Nano-Ti coated with rmBMP-7. For the blood clot groups—on time 0 and on day 5—antibody #13820 detected a nonspecific

band with a lower molecular weight, which was in higher amounts with the presence of MC3T3-E1 cultures (Figure 4C).

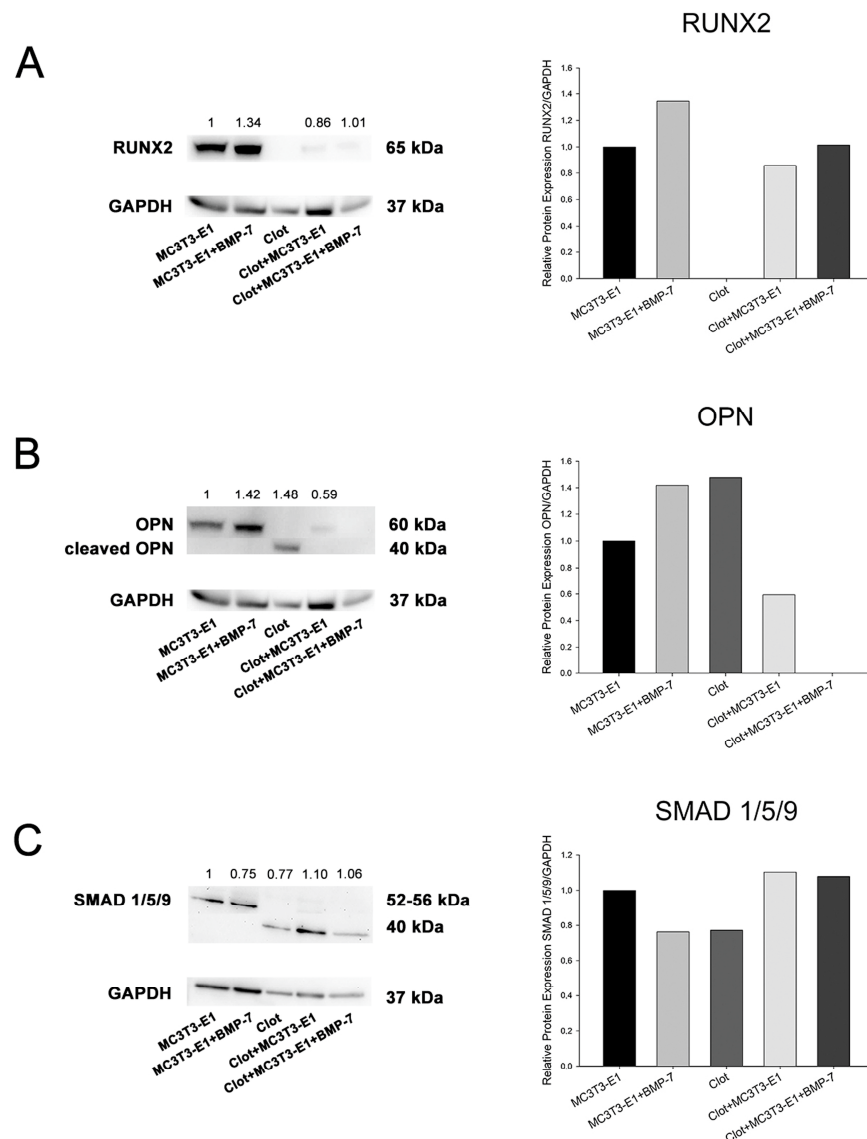


Figure 4. Detection and quantification of RUNX2 (A), OPN (B), and phosphorylated-SMAD 1/5/9 (C) by Western blotting (number of pixels of the protein bands normalized to GAPDH) in MC3T3-E1 cell cultures grown for 5 days and in blood clots on time 0 on Nano-Ti surfaces either functionalized with or without rmBMP-7. The bars represent one biological replicate (resulting from the pooling of 20 independent wells/experimental replicates for each group) and one technical replicate. The ratio of the control group (MC3T3-E1) is assigned a value of 1. Lower molecular weight bands in (B,C) are cropped to fit the figure.

4. Discussion

Our results indicate that the presence of a blood clot has an impact on some key aspects of the interaction of osteoblastic cells with a Ti surface nanotopography functionalized with or without rmBMP-7. There is a tendency towards inhibition of key osteoblast markers relating to mRNA expression, except that of *Opn*. As for the blood clot groups, the functionalization with rmBMP-7 promotes a tendency towards relatively greater osteoblastic differentiation, a finding that is corroborated by RUNX2 protein detection; as for the other proteins evaluated, undetectable levels of OPN and phosphorylated SMAD 1/5/9 are

found in cultures exposed to rmBMP-7. The cleaved form of OPN is only detected in the *in vivo* blood clot prior to MC3T3-E1 cell plating.

Functionalization with rmBMP-7 of Nano-Ti discs not implanted in the animals does not promote osteogenic differentiation of pre-osteoblastic MC3T3-E1 cells during the proliferative phase of cultures. In fact, two out of the six osteoblast markers evaluated—*Bsp* and *Oc*—exhibit a tendency in the order of 20% towards a reduced expression. Because of the 5-day culture time, it is not possible to predict the outcomes of the cultures in terms of osteogenic potential. The surface functionalization with rmBMP-7 likely causes a burst release of the exogenous growth factor, providing an extracellular BMP-7 concentration within the range that has been shown to be inhibitory for osteogenic differentiation [26–28]. However, this simple functionalization strategy must be considered with caution in light of other successful ones using either minimal or much higher concentrations of BMP-7 [8–11]. On the other hand, it permits estimating the challenges that arise when one tries to mimic the interfacial *in vivo* reality for the design of *in vitro* studies on cell response to organic coatings on Ti. Our results highlight that it is feasible to evaluate the interactions of pre-osteoblastic cells with a Ti surface, and likely those with other solid biomaterials, and more closely mimic the *in vivo* reality by integrating a physiological blood clot prior to cell culture.

The strategy to create a hollowed surface on the Nano-Ti disc allows for the formation and stabilization of a blood clot in the mouse dorsal skin dermal tissue model. Epifluorescence and SEM imaging show that structurally, the clot consists of a three-dimensional fibrin network embedding variable amounts of platelets, leukocytes, and erythrocytes, distributed inhomogeneously throughout the surface. Although the combination of nanotopography and hydrophilicity (two surface characteristics of Nano-Ti) [20,21] might contribute to pronounced blood coagulation [29], it has been shown that implant surfaces structured at the micro-scale are more efficient at retaining the fibrin clot, an event that is crucial for bone repair to occur at the tissue–implant interface [30]. Therefore, considering the only occasional occurrence of microtopographic features on the Nano-Ti surface (not shown) and the inhomogeneity of the blood clot on it, it may be more appropriate to hierarchically structure the Ti surface at the micro- and nanoscale [31], or to even functionalize it with a molecule that could contribute to the formation of a more homogenous blood clot/fibrin clot *in vivo*. Either plasma-derived or recombinant fibrinogen might be a good candidate for that purpose.

Irrespective of the presence of rmBMP-7 coating, the observed inhibition of osteoblastic differentiation when MC3T3-E1 cells interact with the physiological blood clot likely reflects the functionality of blood cells and plasma proteins in this model, with synergistic pro-proliferative and/or anti-differentiation effects on pre-osteoblastic cells. More specifically, these effects could be attributed to the degradation rate of fibrin (the main matrix constituent of a blood clot), which impedes osteogenic differentiation under physiological concentrations of fibrinogen and thrombin, as discussed in [32]. *In vitro*, thrombin stimulates osteoblast cell proliferation, migration, and adhesion, and inhibits its differentiation, with effects that are mostly mediated by protease-activated receptor-1, as reviewed in [33]. Moreover, platelets, a major cellular component in blood clots, both trigger thrombin generation [34] and secrete a series of soluble factors that have been shown to inhibit osteoblastic cell differentiation. These include transforming growth factor beta (TGF- β), platelet-derived growth factor (PDGF), and thrombospondin [35–38]. Interestingly, at day 5 of culture, occasional GFP-positive leukocytes derived from blood clots are still observed and intermingled with MC3T3-E1 cells. This observation reveals a somewhat similar occurrence of the complex interplay between the immune system and bone cells that regulates osteoblastic cells at the onset of bone repair by transiently promoting their proliferation while limiting their differentiation, as reviewed in [39,40].

Contrarily to the other osteoblast markers studied, *Opn* expression tends to be upregulated in MC3T3-E1 cells grown on blood clots compared with those grown directly on Nano-Ti. Although it is well known that the overexpression of *Opn* inhibits osteoblast dif-

ferentiation [41], this finding is of particular interest in the context of our biomimetic model, as the biological functions of OPN protein are largely determined by its proteolytic cleavage by the plasma proteases thrombin and plasmin, among others [42–44]. Interestingly, the cleaved form of OPN is only detected in the blood clot at time zero, prior to MC3T3-E1 cell plating, and is thus associated with the cytoplasmic and extracellular accumulation of the protein (derived either from plasma or cellular secretion) that occurs during blood clot formation in the mouse. For MC3T3-E1 cultures that interact with the blood clot during the 5-day period, full-length OPN is either detected in minimal amounts or is not detectable (for the rmBMP-7-coated Nano-Ti). One possible explanation for the discrepancy between mRNA and protein levels here is that OPN accumulation during the initial hours and days of cultures is limited due to protease activities. In addition, close to day 5 of culture, the absence of the cleaved form of OPN is indicative of protease inactivation [45,46].

Despite the benefits of simulating *in vitro* the initial tissue response to rmBMP-7-functionalized Nano-Ti, particularly including a physiological blood clot on its surface, the experimental model presented here exhibits some methodological challenges that remain to be addressed. Firstly, our strategy to use phosphorylated SMAD 1/5/9 as a marker of BMP/Smad signaling, as discussed in [47], surprisingly results in the detection of a nonspecific band with a lower molecular weight only on the blots related to the blood clot groups. At this point, one cannot rule out the possibility that it represents another SMAD [48] that cross-reacts with antibody #13820 and/or reveals the occurrence of the proteasomal degradation of SMAD 1/5/9 [49]. Secondly, the response of the cell line to the control surfaces is not totally comparable to that of the surfaces previously covered by blood clots. Coating with rmBMP-7 might be subjected to changes in its structure and composition, resulting from desorption events [50] and plasma protease activities [51], among others, while the discs are implanted in the animal. Finally, in order to further improve this biomimetic model, the relative proportions of cells of the osteoblast lineage and blood clot elements that occur *in vivo* at the bone–implant interface should be taken into consideration in order to establish a more realistic initial osteogenic cell population at cell plating.

5. Conclusions

The strategy to more closely simulate the early *in vivo* environment at the Ti interface using physiological blood clot formation reveals major changes at the morphological and molecular levels during the proliferative phase of pre-osteoblastic cell cultures on a nanostructured Ti surface functionalized with or without rmBMP-7. By growing MC3T3-E1 cells in the presence of a functional blood clot structure, osteoblastic differentiation tends to be inhibited, and this inhibition is minimally reverted with rmBMP-7 functionalization. These results highlight the importance of developing *in vitro* methods in studies of biomaterials that come closer to the *in vivo* reality. In addition, they point towards the challenges that arise in the attempt to functionalize Ti surfaces with BMP-7, or even other growth factors or organic molecules, in order to efficiently promote osteogenic differentiation.

Supplementary Materials: The following supporting information can be downloaded at: <https://www.mdpi.com/article/10.3390/biomimetics8010123/s1>, Figure S1: Technical drawing of the modified titanium disc; Figure S2: Certificate of the local animal ethical committee; Figure S3: RNA integrity—Electrophoresis file run summary; Figure S4: RNA integrity—Electropherogram summary; Figure S5: Quantitative mRNA expression—Additional technical replicates.

Author Contributions: Conceptualization, P.T.d.O., E.M.R. and A.N.; methodology, L.R.Z., C.L.A.S., E.M.R., G.V.C., S.S., A.N. and P.T.d.O.; formal analysis/investigation, L.R.Z., C.L.A.S., E.M.R., G.V.C., S.S. and P.T.d.O.; writing—original draft preparation, L.R.Z., S.S., A.N. and P.T.d.O.; writing—review and editing, L.R.Z., S.S., A.N. and P.T.d.O.; visualization, L.R.Z., C.L.A.S., E.M.R., G.V.C., S.S., A.N. and P.T.d.O.; supervision, P.T.d.O.; project administration, P.T.d.O.; funding acquisition, P.T.d.O. All authors have read and agreed to the published version of the manuscript.

Funding: This research was funded by the National Council for Scientific and Technological Development (CNPq, Brazil) (grant number 315266/2020-1 (scholarship on research productivity to P.T.d.O.)), and the State of São Paulo Research Foundation (FAPESP, Brazil) (grant numbers 2017/20157-2 (scientific initiation scholarship to G.C.V.) and 2016/50298-4 (regular project to P.T.d.O.)). This study was financed in part by the Coordenação de Aperfeiçoamento de Pessoal de Nível Superior—Brasil (CAPES) (finance code 001) (grant number 1569214 (PhD scholarship to L.R.Z.)). The overall project was also supported by the Canadian Institute of Health Research (CIHR) and the Natural Sciences and Engineering Research Council of Canada (NSERC, RGPIN-2016-04764), as well as the Network for Oral and Bone Health Research (RSBO). A.N. holds a Canada Research Chair in Calcified Tissues, Biomaterials, and Structural Imaging.

Institutional Review Board Statement: Not applicable.

Data Availability Statement: The data present in this study are available on request from the corresponding author under plausible justification.

Acknowledgments: We thank the Electronic Microscopy Laboratory of the Department of Cellular and Molecular Biology and Pathogenic Bioagents, FMRP-USP, and Ribeirão Preto Blood Center Foundation (FUNDHERP-FMRP-USP). We also thank Roger R. Fernandes and Fabíola S. de Oliveira (FORP-USP) for technical assistance.

Conflicts of Interest: The authors declare no conflict of interest.

References

1. Holmes, C.; Tabrizian, M. Surface Functionalization of Biomaterials. In *Stem Cell Biology and Tissue Engineering in Dental Sciences*; Vishwakarma, A., Sharpe, P., Shi, S., Ramalingam, M., Eds.; Academic Press: Cambridge, MA, USA, 2015; pp. 187–206. ISBN 9780123971579. [[CrossRef](#)]
2. Ferraris, S.; Cazzola, M.; Zuardi, L.R.; de Oliveira, P.T. Metal nanoscale systems functionalized with organic compounds. In *Nanostructured Biomaterials for Regenerative Medicine*; Woodhead Publishing Series in Biomaterials; Guarino, V., Iafisco, M., Spriano, S., Eds.; Woodhead Publishing: Sawston, UK, 2020; pp. 407–436. ISBN 9780081025949. [[CrossRef](#)]
3. Jablonská, E.; Horkavcová, D.; Rohanová, D.; Brauer, D.S. A review of in vitro cell culture testing methods for bioactive glasses and other biomaterials for hard tissue regeneration. *J. Mater. Chem. B* **2020**, *8*, 10941–10953. [[CrossRef](#)] [[PubMed](#)]
4. Anderson, J.M. Future challenges in the in vitro and in vivo evaluation of biomaterial biocompatibility. *Regen. Biomater.* **2016**, *3*, 73–77. [[CrossRef](#)] [[PubMed](#)]
5. Jablonská, E.; Kubásek, J.; Vojtěch, D.; Ruml, T.; Lipov, J. Test conditions can significantly affect the results of in vitro cytotoxicity testing of degradable metallic biomaterials. *Sci. Rep.* **2021**, *11*, 6628. [[CrossRef](#)] [[PubMed](#)]
6. Burkhardt, M.A.; Waser, J.; Milleret, V.; Gerber, I.; Emmert, M.Y.; Foolen, J.; Hoerstrup, S.P.; Schlottig, F.; Vogel, V. Synergistic interactions of blood-borne immune cells, fibroblasts and extracellular matrix drive repair in an in vitro peri-implant wound healing model. *Sci. Rep.* **2016**, *6*, 21071. [[CrossRef](#)]
7. Lackington, W.A.; Fleyshman, L.; Schweizer, P.; Elbs-Glatz, Y.; Guimond, S.; Rottmar, M. The response of soft tissue cells to Ti implants is modulated by blood-implant interactions. *Mater. Today Bio.* **2022**, *15*, 100303. [[CrossRef](#)] [[PubMed](#)]
8. Al-Jarsha, M.; Moulisová, V.; Leal-Egaña, A.; Connell, A.; Naudi, K.B.; Ayoub, A.F.; Dalby, M.J.; Salmerón-Sánchez, M. Engineered coatings for titanium implants to present ultralow doses of BMP-7. *ACS Biomater. Sci. Eng.* **2018**, *4*, 1812–1819. [[CrossRef](#)]
9. Zhou, L.; Wu, J.; Wu, D.; Yu, J. Surface functionalization of titanium with Bmp-7/rgd/hyaluronic acid for promoting osteoblast functions. *J. Biomater. Tissue Eng.* **2019**, *9*, 32–39. [[CrossRef](#)]
10. Nemcakova, I.; Litvinec, A.; Mandys, V.; Potocky, S.; Plencner, M.; Doubkova, M.; Nanka, O.; Olejnickova, V.; Sankova, B.; Bartos, M.; et al. Coating Ti6Al4V implants with nanocrystalline diamond functionalized with BMP-7 promotes extracellular matrix mineralization in vitro and faster osseointegration in vivo. *Sci. Rep.* **2022**, *12*, 5264. [[CrossRef](#)]
11. López-Valverde, N.; Aragonese, J.; López-Valverde, A.; Rodríguez, C.; Aragonese, J.M. Role of BMP-7 on biological parameters osseointegration of dental implants: Preliminary results of a preclinical study. *Front. Bioeng. Biotechnol.* **2023**, *11*, 1153631. [[CrossRef](#)]
12. Zuardi, L.R.; de Oliveira, F.S.; Fernandes, R.R.; Gomes, M.P.O.; Spriano, S.; Nanci, A.; de Oliveira, P.T. Effects of rmBMP-7 on osteoblastic cells grown on a nanostructured titanium surface. *Biomimetics* **2022**, *7*, 136. [[CrossRef](#)]
13. Milleret, V.; Tugulu, S.; Schlottig, F.; Hall, H. Alkali treatment of microrough titanium surfaces affects macrophage/monocyte adhesion, platelet activation and architecture of blood clot formation. *Eur. Cells Mater.* **2011**, *21*, 430–444. [[CrossRef](#)] [[PubMed](#)]
14. Huang, H.H.; Chen, J.Y.; Lin, M.C.; Wang, Y.T.; Lee, T.L.; Chen, L.K. Blood responses to titanium surface with TiO₂ nano-mesh structure. *Clin. Oral Implant. Res.* **2012**, *23*, 379–383. [[CrossRef](#)]
15. Anitua, E.; Prado, R.; Orive, G.; Tejero, R. Effects of calcium-modified titanium implant surfaces on platelet activation, clot formation, and osseointegration. *J. Biomed. Mater. Res. A* **2015**, *103*, 969–980. [[CrossRef](#)] [[PubMed](#)]

16. Kopf, B.S.; Schipanski, A.; Rottmar, M.; Berner, S.; Maniura-Weber, K. Enhanced differentiation of human osteoblasts on Ti surfaces pre-treated with human whole blood. *Acta Biomater.* **2015**, *19*, 180–190. [[CrossRef](#)] [[PubMed](#)]
17. VanZweden, E.; Tolsma, R.; Hung, V.; Awad, P.; Sawyer, R.; Li, Y. The advances of blood clots used as biomaterials in regenerative medicine. *Regen. Med.* **2022**, *17*, 957–969. [[CrossRef](#)] [[PubMed](#)]
18. Monroe, D.M.; Hoffman, M. The clotting system—A major player in wound healing. *Haemophilia* **2012**, *18* (Suppl. 5), 11–16. [[CrossRef](#)]
19. Vetrone, F.; Variola, F.; de Oliveira, P.T.; Zalzal, S.F.; Yi, J.H.; Sam, J.; Bombonato-Prado, K.F.; Sarkissian, A.; Perepichka, D.F.; Wuest, J.D.; et al. Nanoscale oxidative patterning of metallic surfaces to modulate cell activity and fate. *Nano Lett.* **2009**, *9*, 659–665. [[CrossRef](#)]
20. Scannavino, R.C.P.; Riccucci, G.; Ferraris, S.; Duarte, G.L.C.; de Oliveira, P.T.; Spriano, S. Functionalization with polyphenols of a nano-textured Ti surface through a high-amino acid medium: A chemical-physical and biological characterization. *Nanomaterials* **2022**, *12*, 2916. [[CrossRef](#)]
21. de Oliveira, P.T.; Zalzal, S.F.; Beloti, M.M.; Rosa, A.L.; Nanci, A. Enhancement of in vitro osteogenesis on titanium by chemically produced nanotopography. *J. Biomed. Mater. Res. A* **2007**, *80*, 554–564. [[CrossRef](#)]
22. Guadarrama Bello, D.; Fouillen, A.; Badia, A.; Nanci, A. A nanoporous titanium surface promotes the maturation of focal adhesions and formation of filopodia with distinctive nanoscale protrusions by osteogenic cells. *Acta Biomater.* **2017**, *60*, 339–349. [[CrossRef](#)]
23. Guadarrama Bello, D.; Fouillen, A.; Badia, A.; Nanci, A. Nanoporosity Stimulates Cell Spreading and Focal Adhesion Formation in Cells with Mutated Paxillin. *ACS Appl. Mater. Interfaces* **2020**, *12*, 14924–14932. [[CrossRef](#)]
24. Bueno, R.B.; Teixeira, L.N.; De Almeida, A.L.; Soares, A.C.; Beloti, M.M.; Sverzut, C.E.; De Oliveira, O.N.; Nanci, A.; Rosa, A.L.; de Oliveira, P.T. Growth and differentiation factor 5 (GDF-5)-functionalized, nanostructured titanium surfaces: In vitro and in vivo studies. In Proceedings of the 10th World Biomaterials Congress, Montréal, QC, Canada, 17–22 May 2016. [[CrossRef](#)]
25. Livak, K.J.; Schmittgen, T.D. Analysis of relative gene expression data using real-time quantitative PCR and the 2(-Delta Delta C(T)). *Methods* **2001**, *25*, 402–408. [[CrossRef](#)] [[PubMed](#)]
26. Maliakal, J.C.; Asahina, I.; Hauschka, P.V.; Sampath, T.K. Osteogenic protein-1 (BMP-7) inhibits cell proliferation and stimulates the expression of markers characteristic of osteoblast phenotype in rat osteosarcoma (17/2.8) cells. *Growth Factors* **1994**, *11*, 227–234. [[CrossRef](#)] [[PubMed](#)]
27. Zhang, F.; Ren, L.F.; Lin, H.S.; Yin, M.N.; Tong, Y.Q.; Shi, G.S. The optimal dose of recombinant human osteogenic protein-1 enhances differentiation of mouse osteoblast-like cells: An in vitro study. *Arch. Oral Biol.* **2012**, *57*, 460–468. [[CrossRef](#)] [[PubMed](#)]
28. Baranowski, A.; Klein, A.; Ritz, U.; Ackermann, A.; Anthonissen, J.; Kaufmann, K.B.; Brendel, C.; Götz, H.; Rommens, P.M.; Hofmann, A. Surface Functionalization of Orthopedic Titanium Implants with Bone Sialoprotein. *PLoS ONE* **2016**, *11*, e0153978. [[CrossRef](#)] [[PubMed](#)]
29. Kopf, B.S.; Ruch, S.; Berner, S.; Spencer, N.D.; Maniura-Weber, K. The role of nanostructures and hydrophilicity in osseointegration: In-vitro protein-adsorption and blood-interaction studies. *J. Biomed. Mater. Res. A* **2015**, *103*, 2661–2672. [[CrossRef](#)]
30. Di Iorio, D.; Traini, T.; Degidi, M.; Caputi, S.; Neugebauer, J.; Piattelli, A. Quantitative evaluation of the fibrin clot extension on different implant surfaces: An in vitro study. *J. Biomed. Mater. Res. B Appl. Biomater.* **2005**, *74*, 636–642. [[CrossRef](#)]
31. Souza, J.C.M.; Sordi, M.B.; Kanazawa, M.; Ravindran, S.; Henriques, B.; Silva, F.S.; Aparicio, C.; Cooper, L.F. Nano-scale modification of titanium implant surfaces to enhance osseointegration. *Acta Biomater.* **2019**, *94*, 112–131. [[CrossRef](#)]
32. Bujoli, B.; Scimeca, J.C.; Verron, E. Fibrin as a Multipurpose Physiological Platform for Bone Tissue Engineering and Targeted Delivery of Bioactive Compounds. *Pharmaceutics* **2019**, *11*, 556. [[CrossRef](#)]
33. Pagel, C.N.; Sivagurunathan, S.; Loh, L.H.; Tudor, E.M.; Pike, R.N.; Mackie, E.J. Functional responses of bone cells to thrombin. *Biol. Chem.* **2006**, *387*, 1037–1041. [[CrossRef](#)]
34. Altman, R.; Scazzioti, A.S.; Herrera, M.D.L.; Gonzalez, C. Thrombin generation by activated factor VII on platelet activated by different agonists. Extending the cell-based model of hemostasis. *Thromb. J.* **2006**, *4*, 5. [[CrossRef](#)] [[PubMed](#)]
35. Maeda, S.; Hayashi, M.; Komiya, S.; Imamura, T.; Miyazono, K. Endogenous TGF-beta signaling suppresses maturation of osteoblastic mesenchymal cells. *EMBO J.* **2004**, *23*, 552–563. [[CrossRef](#)] [[PubMed](#)]
36. de Oliveira, P.T.; de Oliva, M.A.; Maximiano, W.M.; Sebastião, K.E.; Crippa, G.E.; Ciancaglini, P.; Beloti, M.M.; Nanci, A.; Rosa, A.L. Effects of a mixture of growth factors and proteins on the development of the osteogenic phenotype in human alveolar bone cell cultures. *J. Histochem. Cytochem.* **2008**, *56*, 629–638. [[CrossRef](#)] [[PubMed](#)]
37. Bailey Dubose, K.; Zayzafoon, M.; Murphy-Ullrich, J.E. Thrombospondin-1 inhibits osteogenic differentiation of human mesenchymal stem cells through latent TGF-β activation. *Biochem. Biophys. Res. Commun.* **2012**, *422*, 488–493. [[CrossRef](#)]
38. Wu, Y.; Zhang, Y.; Yin, Q.; Xia, H.; Wang, J. Platelet-derived growth factor promotes osteoblast proliferation by activating G-protein-coupled receptor kinase interactor-1. *Mol. Med. Rep.* **2014**, *10*, 1349–1354. [[CrossRef](#)]
39. Lorenzo, J.; Horowitz, M.; Choi, Y. Osteoimmunology: Interactions of the bone and immune system. *Endocr. Rev.* **2008**, *29*, 403–440. [[CrossRef](#)]
40. Yang, N.; Liu, Y. The Role of the Immune Microenvironment in Bone Regeneration. *Int. J. Med. Sci.* **2021**, *18*, 3697–3707. [[CrossRef](#)]
41. Huang, W.; Carlsen, B.; Rudkin, G.; Berry, M.; Ishida, K.; Yamaguchi, D.T.; Miller, T.A. Osteopontin is a negative regulator of proliferation and differentiation in MC3T3-E1 pre-osteoblastic cells. *Bone* **2004**, *34*, 799–808. [[CrossRef](#)]

42. Senger, D.R.; Perruzzi, C.A.; Papadopoulos-Sergiou, A.; Van de Water, L. Adhesive properties of osteopontin: Regulation by a naturally occurring thrombin-cleavage in close proximity to the GRGDS cell-binding domain. *Mol. Biol. Cell* **1994**, *5*, 565–574. [[CrossRef](#)]
43. Agnihotri, R.; Crawford, H.C.; Haro, H.; Matrisian, L.M.; Havrda, M.C.; Liaw, L. Osteopontin, a novel substrate for matrix metalloproteinase-3 (stromelysin-1) and matrix metalloproteinase-7 (matrilysin). *J. Biol. Chem.* **2001**, *276*, 28261–28267. [[CrossRef](#)] [[PubMed](#)]
44. Christensen, B.; Schack, L.; Klänning, E.; Sørensen, E.S. Osteopontin is cleaved at multiple sites close to its integrin-binding motifs in milk and is a novel substrate for plasmin and cathepsin D. *J. Biol. Chem.* **2010**, *285*, 7929–7937. [[CrossRef](#)] [[PubMed](#)]
45. Licari, L.G.; Kovacic, J.P. Thrombin physiology and pathophysiology. *J. Vet. Emerg. Crit. Care* **2009**, *19*, 11–22. [[CrossRef](#)]
46. Kremers, R.M.; Wagenvoort, R.J.; Hemker, H.C. The effect of fibrin(ogen) on thrombin generation and decay. *Thromb. Haemost.* **2014**, *112*, 486–494. [[CrossRef](#)]
47. Guo, J.; Lin, Q.; Shao, Y.; Rong, L.; Zhang, D. BMP-7 suppresses excessive scar formation by activating the BMP-7/Smad1/5/8 signaling pathway. *Mol. Med. Rep.* **2017**, *16*, 1957–1963. [[CrossRef](#)] [[PubMed](#)]
48. Gruendler, C.; Lin, Y.; Farley, J.; Wang, T. Proteasomal degradation of Smad1 induced by bone morphogenetic proteins. *J. Biol. Chem.* **2001**, *276*, 46533–46543. [[CrossRef](#)] [[PubMed](#)]
49. Zhu, H.; Kavsak, P.; Abdollah, S.; Wrana, J.L.; Thomsen, G.H. A SMAD ubiquitin ligase targets the BMP pathway and affects embryonic pattern formation. *Nature* **1999**, *400*, 687–693. [[CrossRef](#)]
50. Dong, X.; Wang, Q.; Wu, T.; Pan, H. Understanding adsorption-desorption dynamics of BMP-2 on hydroxyapatite (001) surface. *Biophys. J.* **2007**, *93*, 750–759. [[CrossRef](#)]
51. Wagner, I.; Wang, H.; Weissert, P.M.; Straube, W.L.; Shevchenko, A.; Gentzel, M.; Brito, G.; Tazaki, A.; Oliveira, C.; Sugiura, T.; et al. Serum proteases potentiate BMP-induced cell cycle re-entry of dedifferentiating muscle cells during newt limb regeneration. *Dev. Cell* **2017**, *40*, 608–617.e6. [[CrossRef](#)]

Disclaimer/Publisher’s Note: The statements, opinions and data contained in all publications are solely those of the individual author(s) and contributor(s) and not of MDPI and/or the editor(s). MDPI and/or the editor(s) disclaim responsibility for any injury to people or property resulting from any ideas, methods, instructions or products referred to in the content.